

# The Hierarchical Nature of the Spin Alignment of Dark Matter Haloes in Filaments

M.A. Aragon-Calvo<sup>1\*</sup>

<sup>1</sup>*The Johns Hopkins University, 3400 Charles St., Baltimore, MD, USA.*

10 April 2021

## ABSTRACT

Dark matter haloes in cosmological filaments and walls have their spin vector aligned (in average) with their host structure. While haloes in walls are aligned with the plane of the wall independently of their mass, haloes in filaments present a mass dependent two-regime orientation. Here we show that the transition mass determining the change in the alignment regime (from parallel to perpendicular) depends on the hierarchical level in which the halo is located, reflecting the hierarchical nature of the Cosmic Web. By explicitly exposing this hierarchy we are able to identify the contributions of different components of the filament network to the spin alignment signal. We discuss a unifying picture to describe the alignment of haloes in filaments and walls consistent with previous results and our findings based on a two-phase angular momentum acquisition, first via tidal torquing and later via anisotropic mass accretion.

The hierarchical identification and characterization of cosmic structures was done with a new implementation of the Multiscale Morphology Filter. The MMF-2 (introduced here) represents a significant improvement over its predecessor in terms of robustness and by explicitly describing the hierarchical relations between the elements of the Cosmic Web.

**Key words:** Cosmology: large-scale structure of Universe; methods: data analysis, N-body simulations

## 1 INTRODUCTION

In the gravitational instability scenario galaxies acquire their angular momentum via tidal torque produced by a misalignment between the inertia tensor of the proto-halo and the embedding gravitational shear tensor generated by the surrounding matter distribution. This is the so called Tidal Torque Theory (TTT) (Hoyle 1951; White 1984). Although the TTT predicts a correlation between the spin orientation of galaxies and their local Large Scale Structure observations of spin alignments have been so far inconclusive and often contradictory (Kashikawa & Okamura (1992); Navarro et al. (2004); Patiri et al. (2006); Trujillo et al. (2006); Lee & Erdogdu (2007); Brunino et al. (2007); Jones et al. (2010); Varela et al. (2012); Tempel et al. (2013) among others). The reason is still not clear and may include the intrinsic difficulties in deducing the spin vector of galaxies, small galaxy samples, challenges in characterizing LSS from galaxy redshift catalogues, etc.

On the theoretical/numerical front the picture is more clear. To date there is a consensus that the spin vector of haloes in walls lies in the plane of their host walls while haloes in filaments have their spin either parallel or perpendicular to their host filament depending on their mass (Aragón-Calvo et al. 2007; Hahn et al. 2007; Zhang et al. 2009; Codis et al. 2012; Trowland et al. 2013; Libeskind et al. 2013). An important aspect of the spin alignment of haloes in filaments is the existence of a transition mass  $M_{tr}$ , at which haloes change their orientation from parallel to perpendicular. This effect was first reported by Aragón-Calvo et al. (2007) and later confirmed by other authors (Hahn et al. 2007; Zhang et al. 2009; Codis et al. 2012; Trowland et al. 2013; Libeskind et al. 2013). The spin alignment of low-mass haloes also has a redshift dependence starting perpendicular and becoming parallel at  $z \sim 1$  (Aragón-Calvo et al. 2007; Trowland et al. 2013). This common primordial orientation and subsequent change indicates an additional mechanism for angular momentum acquisition that has a stronger effect in low-mass haloes. In the observational front the two regimes of alignment/anti-alignment

\* E-mail:miguel@pha.jhu.edu

of low-mass and high-mass haloes in filaments have been recently observed by Tempel et al. (2013) if one assumes a correlation between Hubble type and galaxy/halo mass. They found that bright spirals have a weak tendency to have their spin parallel to their host filaments while Elliptical/S0 show a strong perpendicular alignment.

The existence of a hierarchy of structures in the Cosmic Web in which large structures contain and are defined by smaller ones (Sheth & van de Weygaert (2004); Einasto et al. (2011); Aragon-Calvo & Szalay (2013) among others) begs the question of whether the halo alignment reflects this hierarchy. The limited number of studies that link the alignment signal and the hierarchy of cosmic structures indicate that the transition mass of alignment in filaments depends on the scale of the filament (Codis et al. 2012) and the distance from the halo to the closest cluster (Zhang et al. 2009). However, to date no direct link has been established between halo alignment and the hierarchy of cosmic structures.

The TTT theory does not provide a mechanism (at least a simple one) to produce the observed two-regime alignment of haloes with their mass or to change the alignment of haloes from perpendicular to parallel with time. Recently an alternative mechanism for angular momentum acquisition has been discussed by Libeskind et al. (2012); Codis et al. (2012) and Trowland et al. (2013) in which angular momentum is generated by the anisotropic infall of matter. This is in term defined by the surrounding LSS morphology and dynamics, offering a natural process for spin-LSS correlations. This secondary-torque mechanism may help explain the change in alignment and possibly even contribute to the primordial torque generation.

## 2 MMF-2: HIERARCHICAL IDENTIFICATION OF FILAMENTS AND WALLS

In order to study the effect of environment in the alignment of haloes in filaments and walls we need to characterize the density field according to its local geometry, compute its local direction and, for the problem at hand, its *hierarchical relations*. The identification of filaments and walls was performed using a significantly improved implementation of the Multiscale Morphology Filter (MMF, Aragón-Calvo et al. (2007)). The MMF-2 performs the identification of structures on a generalization of scale-space: the hierarchical-space, which exposes the *hierarchical character* of the density field in contrast to the scale-space approach (as in the original MMF and its derived implementations (Zhang et al. 2009; Cautun et al. 2013)) which emphasize the *scale* of the structures and is insensitive to their nesting relations. The hierarchical space used in the MMF describes both scale and nesting relations.

We generate the hierarchical space as described in Aragon-Calvo et al. (2010b) and Aragon-Calvo (2012), by Gaussian-smoothing the *initial conditions* instead of the *final* density field as in the scale-space approach. This *linear-regime smoothing* is applied when all Fourier modes are independent, allowing us to target specific scales in the density field before Fourier mode-mixing occurs. The smooth initial conditions evolve by gravity producing all the anisotropic features of the Cosmic Web but lacking of small-scale struc-

tures including dense haloes (below the smoothing scale). This reduces the dynamic range in the density field and greatly limits the contamination produced by dense haloes in the identification of filaments and walls.

The identification of structures in the original MMF method and the one presented here is done based on the second-order local variations of the density field encoded in the Hessian matrix. LSS morphologies are associated to ratios between the eigenvalues of the Hessian matrix ( $\lambda_1 < \lambda_2 < \lambda_3$ , see Aragón-Calvo et al. (2007)). The output of the MMF-2 is a set of “masks” sampled on a regular grid indicating which voxels belong to a given morphology at a given hierarchical level. For our purposes we generated a filament, sub-filament wall and sub-wall masks ( $F_1$ ,  $F_2$ ,  $W_1$  and  $W_2$  respectively, the subscript indicates the hierarchical level). These masks roughly correspond to the “feature maps”  $\mathcal{F}$  in the original MMF algorithm. A complete description of the MMF-2 method will be presented in Aragon-Calvo (2013) in preparation.

## 3 N-BODY SIMULATION AND DM HALOES

The N-body simulations and related halo catalogues used in this work are based on the MIP correlated ensemble simulation. (Aragon-Calvo 2012). The MIP simulation consists of 220 realizations sharing identical LSS fluctuations defined at  $k < k_{\text{cut}}$  where  $k_{\text{cut}}$  corresponds to a scale of 4 Mpc  $h^{-1}$ . At smaller scales ( $k > k_{\text{cut}}$ ) realizations can be considered independent between each other. Each realization in the ensemble contains  $256^3$  dark matter particles inside a box of 32 Mpc  $h^{-1}$  of side with cosmological parameters  $\Omega_m = 0.3$ ,  $\Omega_\Lambda = 0.7$ ,  $h = 0.73$ ,  $\sigma_8 = 0.8$ .

### 3.1 Hierarchical space

For the purpose of this paper we generated a two-level hierarchical space defined by linear-regime smoothing scales of 4 and 2 Mpc  $h^{-1}$  delineating the prominent structures in the Cosmic Web and their substructure respectively. We denote these hierarchical levels as LEV-1 (filaments/walls) and LEV-2 (sub-filaments/sub-walls). From the template initial conditions used to generate the MIP ensemble (see Aragon-Calvo (2012) for details) we generated low-resolution  $128^3$  initial conditions grids and smoothed them at the scales defined above. We then evolved the particles to the present time  $z = 0$  using the PM-Tree code GADGET-2 (Springel 2005). These simulation were used only to compute density fields.

### 3.2 Density fields

From the particle distribution we computed densities following the technique presented in Abel et al. (2012) and Shandarin et al. (2012). In this novel approach particles define Lagrangian volumes that reflect the changes in density as particles evolve deforming the original volume. Lagrangian volumes are defined by 8 adjacent particles forming a “cube” that is divided into 6 tetrahedra. We estimate densities in the tessellation as the mean density of the adjacent tetrahedra to each vertex and interpolated to a regular grid taking care to account for multistreams. This method makes

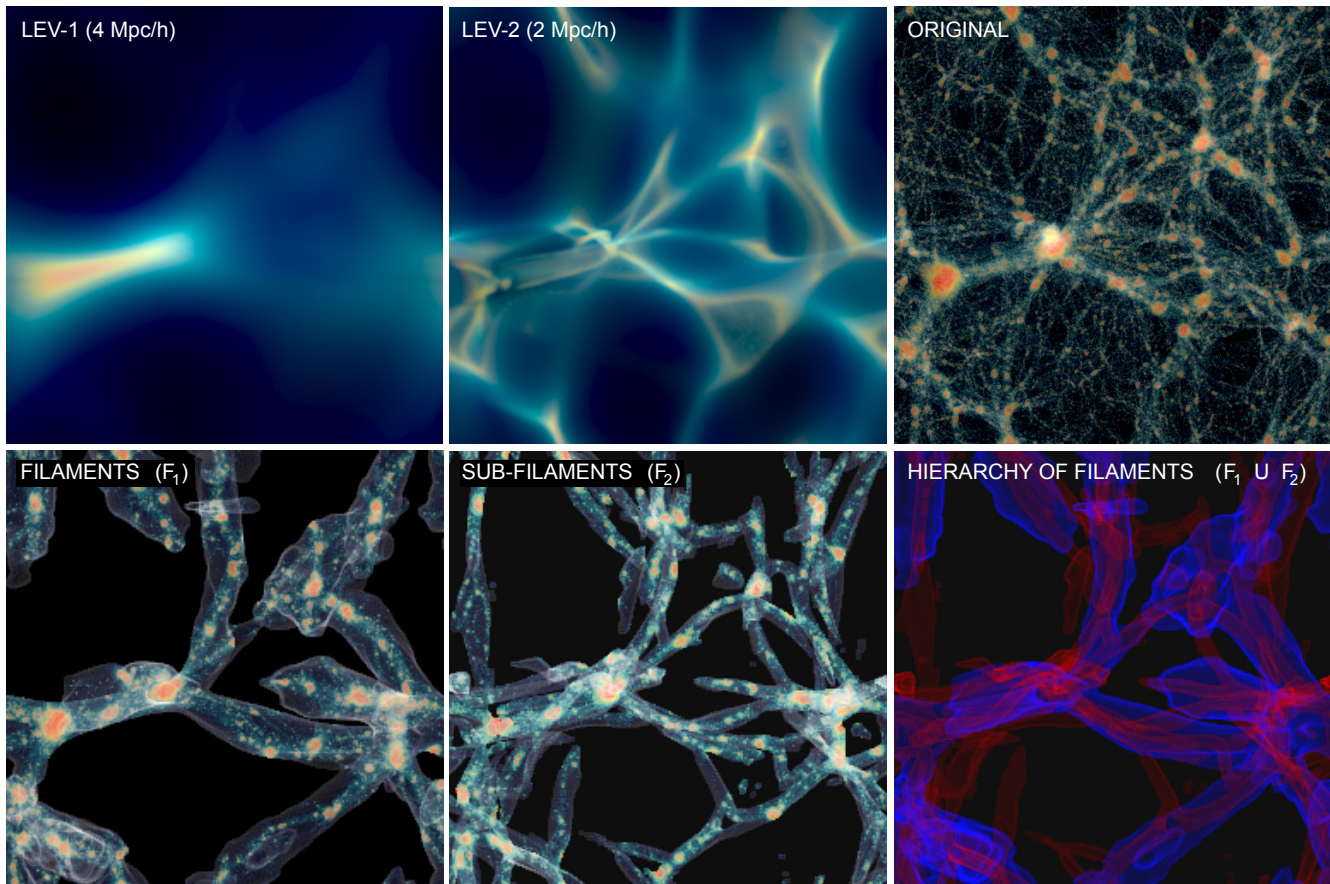


**Figure 1.** The MMF-2 method. Top panels: hierarchical space. We show the volume rendering of the density field at  $z = 0$  for linear-regime smoothing at 4, 2 Mpc  $h^{-1}$  and no smoothing (left, center and right panels respectively). The thickness of the slices was chosen to show as many structures as possible while avoiding confusion. Bottom panels: Hierarchical identification of filaments. The left and center panels show the density field inside filaments ( $F_1$ ) and sub-filaments ( $F_2$ ) respectively. We highlight the filament mask as a semitransparent surface. The hierarchy of filaments (blue) and sub-filaments (red) is shown in the bottom right panel.

density estimation computationally straightforward, it produces a continuous volume-filling density field with practically no artifacts in low and medium-density regions (our regions of interest) and is self-adaptive by construction.

### 3.3 Halos

Haloes were identified in each realization of the MIP ensemble using the friends-of-friends algorithm with a linking parameter  $b = 0.2$ . We imposed a count limit of 50 particles corresponding to a halo mass of  $\sim 8 \times 10^9 M_\odot h^{-1}$ . We use the MIP ensemble in “stack mode”, where halo catalogues from all realizations are aggregated into one “master halo catalogue”. The full MIP stacked ensemble contains  $\sim 5 \times 10^6$  haloes inside a volume of  $(32 \text{ Mpc } h^{-1})^3$  giving unprecedented halo number density. For each FoF group, we compute its mass, center of mass, mean velocity etc. The angular momentum was computed as:

$$\mathbf{J} = \sum_i^N m_i \mathbf{r}_i \times (\mathbf{v}_i - \bar{\mathbf{v}}), \quad (1)$$

where the sum is over all the particles in the halo,  $m_i$  is the particle mass,  $\mathbf{r}_i$  is the distance to each particle from the center of the halo,  $\mathbf{v}_i$  is the peculiar velocity of the particle

and  $\bar{\mathbf{v}}$  the mean velocity of the halo with respect to its center of mass.

### 3.4 Spin alignment in filaments and walls

The angle between the spin of the halo and its host filament or wall was computed as  $\theta_F = \phi_W$  and  $\theta_W = 90^\circ - \phi_W$ , where  $\phi_F = |\cos^{-1}(\mathbf{J} \cdot \lambda_1)|$  and  $\phi_W = |\cos^{-1}(\mathbf{J} \cdot \lambda_3)|$  are the angles between the spin of the halo and the direction of its host filament ( $\lambda_1$  corresponding to the direction of constant density along the filament’s axis) or the normal to the wall ( $\lambda_3$  corresponding to the direction of maximum change in the density field).

### 3.5 The filament/sub-filament sample

Figure 1 shows the density field at  $z = 0$  from the two hierarchical levels defined by 4 and 2 Mpc  $h^{-1}$  linear-regime smoothing (LEV-1 and LEV-2 respectively) and the original initial conditions with no smoothing (top panels from left to right). The original density field enclosed in the filament and sub-filament mask is shown at the bottom-left and center panels. The two-level hierarchy of filaments (the union of the two sets) is shown in the bottom-right panel.

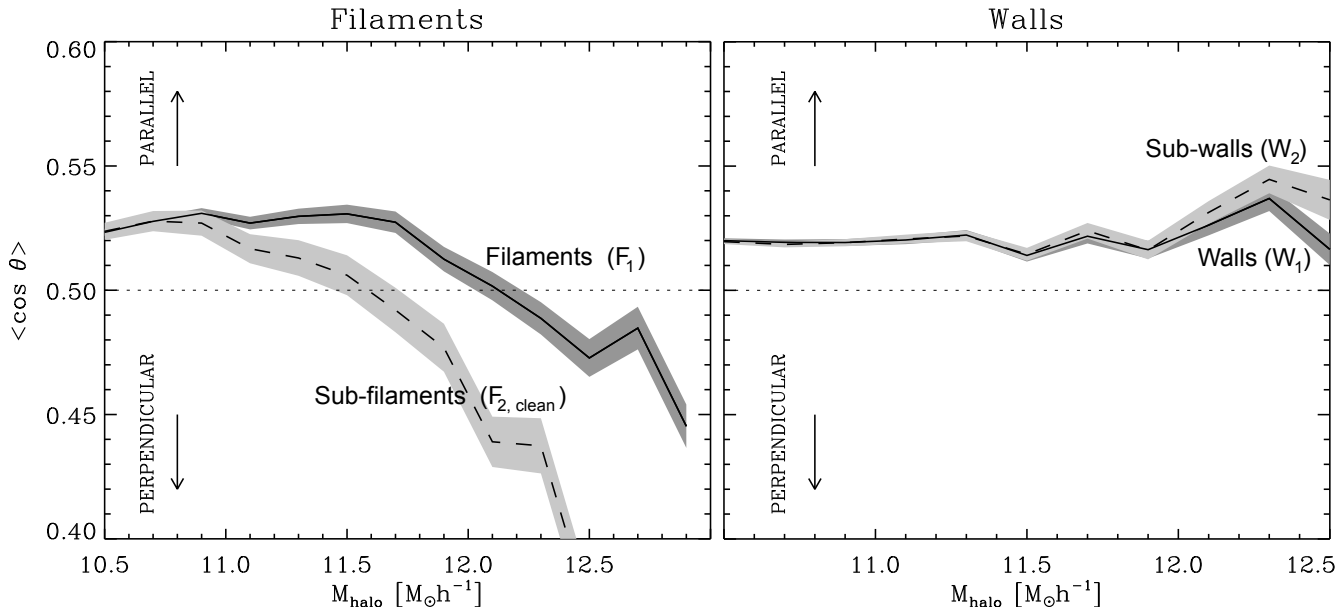


**Figure 2.** Spin alignment of haloes as function of mass in filaments (left panel) and walls (right panel). The alignment is measured with the mean  $\cos \theta$  where 0.5 corresponds to no preferred alignment. The sample was divided in haloes in filaments/walls (solid lines) and sub-filaments/sub-walls (dashed lines). Error bars per bin were computed from 1000 random realizations with the same number of points as their corresponding bin.

In order to clearly differentiate between the alignment signal of haloes in filaments and sub-filaments we “cleaned” the sub-filament mask by removing the sub-filaments embedded inside filaments. We also constrained sub-filaments to be contained by walls. This removes the tenuous intra-void filaments. The mask of “clean” sub-filaments is then defined as:

$$F_{2,\text{clean}} = F_2 \cap W_1 \cap F_1^c \quad (2)$$

where  $F_2$  is the sub-filament mask,  $W_1$  is the wall mask and  $F_1^c$  is the complement of the filament mask. In what follows  $F_1$  and  $F_{2,\text{clean}}$  denote the masks we used to compute spin-alignment of haloes in filaments and sub-filaments respectively

## 4 RESULTS

Our main findings are shown in Figure 2 where we measure the mean cosine of the angle between the spin vector of haloes and the direction of their host filament/sub-filament (left panel) or wall/sub-wall (right panel) as a function of halo mass. A more detailed view of the spin alignment distribution for haloes in filaments/sub-filaments is shown in Figure 3. Our results can be summarized as follows:

- Haloes in filaments and sub-filaments present a two-regime spin alignment as a function of their mass: low-mass haloes are (in average) aligned parallel to their parent filament while high-mass haloes are oriented perpendicular to it, confirming previous findings.
- The mean alignment of low-mass haloes seems to converge at  $\langle \cos \theta \rangle \sim 0.53$  down to a halo mass of  $\sim 10^{10} M_{\odot} h^{-1}$  in both filaments and sub-filaments.
- The alignment of high-mass haloes does not seem to

converge like in the case of the low-mass haloes. Instead, the alignment signal increases with increasing mass.

- We found a significant difference in the transition mass  $M_{\text{tr}}$  dividing parallel and perpendicular alignment for haloes in filaments and sub-filaments being  $M_{\text{tr,low}} \sim 1.5 \times 10^{12} M_{\odot} h^{-1}$  and  $M_{\text{tr,high}} \sim 4 \times 10^{11} M_{\odot} h^{-1}$  respectively.
- The slope in the alignment-mass curve of high-mass haloes in sub-filaments is more pronounced than in the case of haloes in filaments.
- Haloes in walls/sub-walls have their spin oriented in the plane of the wall for the full range of masses in our halo sample ( $\sim 10^{10} - 10^{12.5} M_{\odot} h^{-1}$ ).
- While the spin alignment distribution of haloes in filaments and sub-filaments seem scaled versions of each other (see Figure 3) the spin alignment distribution of low-mass haloes is practically the same for filaments and sub-filaments even though their transition masses are different by a factor of 3.

## 5 CONCLUSIONS AND DISCUSSION

Using an advanced LSS classification algorithm (MMF-2) and a novel N-body correlated ensemble simulation we were able to measure the halo spin alignment signal with unprecedented detail in a variety of cosmic environments. Our results confirm previous findings while significantly improving the alignment signal detection. However, we found a difference in the transition mass  $M_{\text{tr}}$  at which the spin alignment changes from being parallel (low-mass haloes) to perpendicular (high-mass haloes) depending on the hierarchical level of the host filament. This hierarchy-dependent effect has not been observed before due to the inability to explicitly target the nesting relations of the structures in the Cosmic Web.

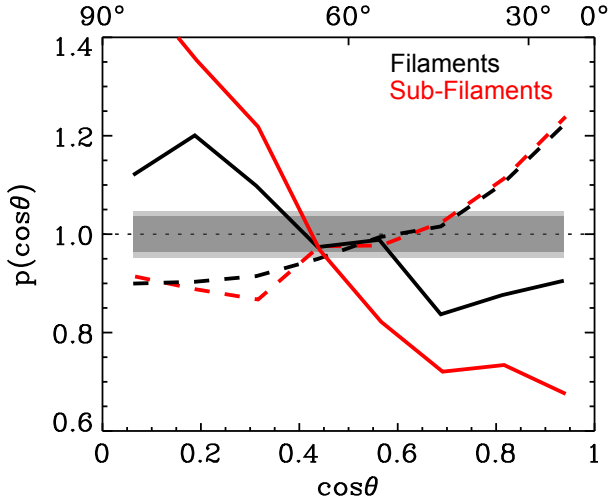


**Figure 3.** Distribution of angles between the spin of a halo and its parent filament (black line) or sub-filament (red line). The samples were divided as high-mass haloes (solid line) and low-mass haloes (dashed line). The transition mass for filaments and sub-filaments corresponds to  $6 \times 10^{11}$  and  $2 \times 10^{12} M_{\odot} h^{-1}$  respectively.

We found that haloes in walls have their spine aligned with the plane of the wall independently of the halo’s mass.

The explicit link between halo spin alignment and Cosmic Web hierarchy was possible with the use of the MMF-2 method (introduced here) that identifies cosmic structures and their hierarchical relations and benefits from an improved density estimation algorithm. The use of the MIP simulation allowed us to perform a high-resolution analysis of the density field over a relatively small volume while at the same time providing us with the large number of haloes needed to detect the spin alignment signal.

### 5.1 On the origin and fate of the spin alignment

The change of alignment of haloes in filaments, the dependence of the transition mass with redshift (Codis et al. 2012) and filament hierarchy (this work) indicates a “secondary torque” process that acts cumulatively and affects all haloes but manifest itself first in low-mass haloes. Since tidal torque is mostly efficient before turnaround the process changing the spin orientation of haloes must be of a different nature. The anisotropic infall scenario offers a tantalizing alternative. Walls and sub-walls accrete mass from their adjacent voids in the direction parallel to the normal of the wall inducing angular momentum on the plane of the wall so haloes retain their primordial spin alignment. On the other hand filaments and sub-filaments accrete mass mainly from their adjacent walls in the direction perpendicular to the filament thus inducing a parallel spin alignment. Low mass haloes are more affected because their low-mass makes them prone to have their spin direction changed for a given mass accretion rate compared to high-mass haloes. The stronger perpendicular alignment of haloes in sub-filaments in comparison to haloes in filaments reflects the more quiet environment characteristic of walls and their embedded sub-filaments. This is a natural consequence of the hierarchy of the Cosmic Web.

## 6 ACKNOWLEDGEMENTS

This research was funded by the Betty and Gordon Moore Foundation and a “New Frontiers of Astronomy and Cosmology” grant from the Sir John Templeton Foundation. The author would like to thank Mark Neyrinck, Xin Wang, Lin Yang and Alex Szalay for stimulating discussions.

## REFERENCES

- Abel, T., Hahn, O., & Kaehler, R. 2012, MNRAS, 427, 61  
 Aragón-Calvo, M. A., van de Weygaert, R., Jones, B. J. T., & van der Hulst, J. M. 2007a, ApJL, 655, L5  
 Aragón-Calvo, M. A., Jones, B. J. T., van de Weygaert, R., & van der Hulst, J. M. 2007b, A&A, 474, 315  
 Aragón-Calvo, M. A., 2007c, PhD. Thesis, University of Groningen, The Netherlands.  
 Aragón-Calvo, M. A., Platen, E., van de Weygaert, R., & Szalay, A. S. 2010, ApJ, 723, 364  
 Aragón-Calvo, M. A., van de Weygaert, R., Araya-Melo, P. A., Platen, E., & Szalay, A. S. 2010, MNRAS, 404, L89  
 Aragón-Calvo, M. A., Silk, J., & Szalay, A. S. 2011, MNRAS, 415, L16  
 Aragón-Calvo, M. A. 2012, arXiv:1210.7871  
 Aragón-Calvo, M. A., & Szalay, A. S. 2013, MNRAS, 428, 3409  
 Brunino, R., Trujillo, I., Pearce, F. R., & Thomas, P. A. 2007, MNRAS, 375, 184  
 Cautun, M., van de Weygaert, R., & Jones, B. J. T. 2013, MNRAS, 429, 1286  
 Codis, S., Pichon, C., Devriendt, J., et al. 2012, MNRAS, 427, 3320  
 Einasto, J., Huitsi, G., Saar, E., et al. 2011, AAP, 531, A75  
 Hahn, O., Carollo, C. M., Porciani, C., & Dekel, A. 2007, MNRAS, 381, 41  
 Hahn, O., Teyssier, R., & Carollo, C. M. 2010, MNRAS, 405, 274  
 Hoyle, F. 1951, Problems of Cosmical Aerodynamics, 195  
 Jones, B. J. T., van de Weygaert, R., & Aragón-Calvo, M. A. 2010, MNRAS, 408, 897  
 Kashikawa, N., & Okamura, S. 1992, PASJ, 44, 493  
 Lee, J., & Erdogdu, P. 2007, ApJ, 671, 1248  
 Libeskind, N. I., Hoffman, Y., Knebe, A., et al. 2012, MNRAS, 421, L137  
 Libeskind, N. I., Hoffman, Y., Forero-Romero, J., et al. 2013, MNRAS, 428, 2489  
 Navarro J. F., Abadi M. G., Steinmetz M. 2004, ApJL, 613, L41  
 Patiri, S. G., Cuesta, A. J., Prada, F., Betancort-Rijo, J., & Klypin, A. 2006, ApJL, 652, L75  
 Shandarin, S., Habib, S., & Heitmann, K. 2012, PrD, 85, 083005  
 Sheth R. K., van de Weygaert R., 2004, MNRAS, 350, 517  
 Springel V., 2005, MNRAS, 364, 1105  
 Tempel, E., Stoica, R. S., & Saar, E. 2013, MNRAS, 428, 1827  
 Trowland, H. E., Lewis, G. F., & Bland-Hawthorn, J. 2013, ApJ, 762, 72  
 Trujillo, I., Carretero, C., & Patiri, S. G. 2006, ApJL, 640, L111  
 Varela, J., Betancort-Rijo, J., Trujillo, I., & Ricciardelli, E. 2012, ApJ, 744, 82

6 *Aragon-Calvo M.A.*

White S. D. M. 1984, ApJ, 286, 38

Zhang, Y., Yang, X., Faltenbacher, A., et al. 2009, ApJ,  
706, 747